Simulating the Measurement of the Electron Beam Emittance at AWAKE

P. Chin[a], E. Simpson Dore[a], L. Deacon[a], F. Keeble[a], S. Jolly[a], M. Wing[a]

[a] *UCL, Gower Street, London WC1E 6BT, UK*

Abstract

In preparation for runs at AWAKE in CERN simulations of the beam and measurement of the beam with the spectrometer were carried out in order to find how the spectrometer behaved under changes to experimental parameters.

Keywords: plasma wakefield, spectrometer, emittance, electron beam, self-modulation instability

Contents

1. Introduction

Advancements in quantum and particle physics are primarily driven by experimental observations which can verify or refute previous hypotheses, or can provide data from which new hypotheses can be drawn. Particle colliders are a main source of observational data at the quantum scale, and can create millions of collision events every second. Design modifications mostly increase the luminosity of the collision in order to produce more data

Proton–proton beam energies at the Large Hadron Collider (LHC) have recently reached energies of 13 TeV [1], whereas lepton–lepton colliders have yet to reach the TeV energy scale. The largest of which, the Large Electron-Proton Collider (LEP), was closed down to make way for the LHC in 2000 after having reached a maximum energy of 209 GeV [2].

One of the drawbacks to circular accelerators, is the loss of a particle's energy due to synchrotron radiation. This is the emittance of radiation from relativistic charged particles that are moving in a uniform magnetic field. The energy loss is inversely proportional to the fourth power of the rest mass of the particle **??**, meaning that electrons lose more energy than protons by a factor of about 10^{13} which is. During experiments performed at the LEP the radiated power when running at 100 GeV reached about 18 MW which needs to be resupplied to the beam.

There are currently two RF linear lepton accelerator proposals, the Compact Linear Collider (CLIC) and the International Linear Collider (ILC) which are expected to reach collision energies of up to several TeV and 500 GeV respectively. Both collaborations have recently joined efforts under the Linear Collider Collaboration.

Looking further into the future
continuing to increase the energy of colliding beams allows for an increasing number of interactions to be observed.

2. Plasma Wakefield Acceleration

Current radio-frequency (RF) accelerator technology is limited to an electromagnetic gradient of about $100\,\mathrm{MeV\,m^{-1}}$ due to material beakdown in the walls of the structure. The ability of plasma to sustain very large electromagnetic fields made it a good candidate for a medium within which charged particles can be accelerated. In 1979, the concept of laser plasma acceleration was shown in simulations to be of practial use in accelerators and pulsers [3]. More recently, proof-of-concept experiments implementing laser plasma acceleration have been shown to accelerate electrons to the GeV scale in a cm-scale plasma cell [4, 5], showing results that are consistent with simulations.

2.1. Self-modulation instability

The first challenge in the development of this accelerator was getting the length of the proton driver bunch small enough so that resonance occurs with the electrons in the plasma. Typical proton bunches, i.e. those produced by the CERN Super Proton Synchrotron (SPS), have lengths of $\sim$ 10 cm which cannot directly create strong plasma waves at the required wavelength in the mm scale as the Fourier component of the proton beam at the plasma frequency is negligible. Simulations [6] on the compression of these bunches show that reducing the longitudinal phase volume blows up the transverse phase volume. An alternative method would be to split up the proton bunch into a number of micro-bunches to be simultaneously decelerated.

An instability between the beam and the plasma arises from the mutual amplification of the rippling of the beam radius and the plasma wave. This instability tends to destroy the plasma wave as the amplification focuses and defocuses selected slices of the beam. This problem was solved by seeding the self-modulated instability (SMI) with a short electron bunch [7], a laser pulse [8] or a sharp cut in the bunch profile[6]. This will promote a single mode and suppress other modes, including the strongest competing modes, the hosing modes [9] and produce well-separated micro-bunches.

2.2. Uniform-density plasma cell

The plasma wavelength is $\lambda_{pe} \approx 1.26$ mm meaning that the 10 cm proton bunch will have to be split into $\sim$ 100 micro-bunches in order to be able to drive the wake. Each micro-bunch contributes to the wakefield, and only if the plasma density is uniform will the contribution of each bunch be coherent. Incoherence will cause the electron bunches to arrive at the wrong phase in the plasma oscillation. An increase in the plasma density will shorten the plasma wavelength causing the electron bunch to crest plasma wave it was riding and fall into the defocusing phase of the plasma wave as shown in Fig 1(a). A decrease in the plasma density will increase the plasma wavelength causing the plasma wave to fall further behind the electron bunch meaning the electron bunch to fall into the trough of the plasma wave resulting in a deceleration of the electron beam 1(c). The electron beam must be in the region of length $\lambda_{pe}/4$ between the defocusing and decelerating phases of the plasma wave.

This requirement of the plasma limits the plasma selection to being uniform rubidium vapor, ionised by a co-propagating laser pulse [11, 12]. Rubidium was chosen due to it's low ionization potential and heavy atomic mass. A heavy element is required to minimize the movement of the plasma's nuclei which causes adverse effects on the plasma's behaviour [13, 14]. The Rubiduim vapor is kept in thermodynamic equilibrium at a constant temperature and volume.

2.3. Injection of the witness beam

Due to SMI, the shape of the drive beam changes in the plasma and for the first four meters, the difference between the phase velocity of the wakefield and the proton

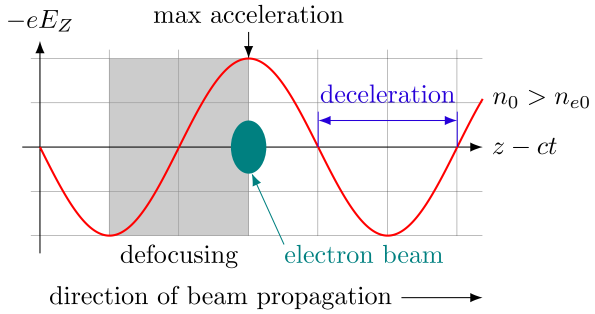

(a) asdkfjasdlfj sdk dfs f

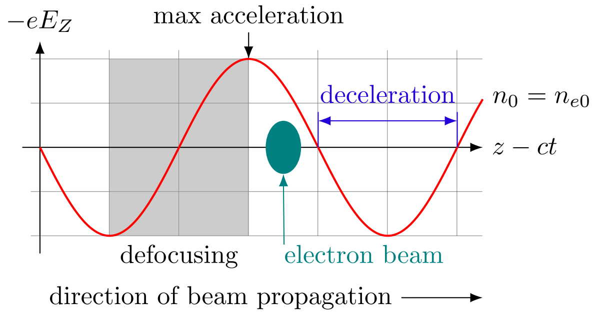

(b) asdkfjasdlfj sdk dfs f

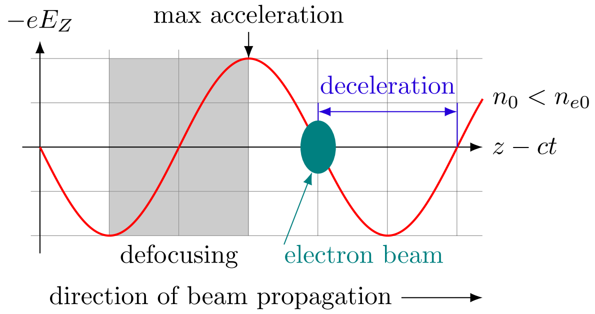

(c) asdkfjasdlfj sdk dfs f

Figure 1: Phasing of the electron bunch for increased density (a) correct density (b) and decreased density (c). [10]

beam velocity is quite large and this will effect the electron beam in the same manner as having a non uniform plasma, detailed above. To avoid this problem it was suggested that the electrons could be injected into the plasma after SMI had fully developed. The design of the injection method arrived at passing the electron beam through a narrow vacuum tube separated from the plasma by a thin foil. Then after $\sim 4\,\mathrm{m}$ the electrons will be directed into the wakefield close close behind the proton driving beam.

3. AWAKE

The aim of this experiment is to provide a proof-of-concept for proton driven plasma wakefield acceleration to be able to accelerate electrons beams to the TeV energy scale. An overview of the experiment as described in the AWAKE design overview: *AWAKE, The Advanced Proton Driven Plasma Wakefield Acceleration Experiment at CERN* [15] is as follows:

The CERN Super Proton Synchrotron (SPS) will provide a 400 GeV proton beam with a bunch length of $\sigma_z = 12\,\mathrm{cm}$ and an intensity of $\sim 3 \times 10^{11}$ protons per bunch. This will travel down the 750 m long proton beam line, previously used for the CERN Neutrinos to Gran Sasso project (CNGS), and be focused to a horizontal and vertical rms size $\sigma_{x,y} = 200\,\mu\mathrm{m}$ before entering a 10 m long Rubiduim vapor plasma cell with an adjustable density at the 10^{14} to 10^{15} electrons/cm scale.

The proton driver will self modulate at the plasma wavelength λ_{pe} after being seeded by a high powered $\approx 4.5\,\mathrm{TW}$ laser pulse that is co-axial and co-propagating with the proton driver beam. This laser also serves the purpose of ionising the Rubidium vapor to create the plasma. For these beams to be co-axial for the full length of the plasma cell, they need to be synchronous to within 100 ps and the size of the focal point of the proton beam is required to be $\leq 100\,\mu\mathrm{m}$ and $\leq 15\,\mu\mathrm{rad}$

The electron witness beam will be created via photo-emission by an illuminating cathode electron source and accelerated by a 2.5 cell RF-gun and a meter long booster at 3 GHz.

4. Spectrometer

There are two main goals the spectrometer is expected to fulfill. The first is to measure the mean energy and energy spread of the beam. Is it this measurement of the mean energy that determines the success of the AWAKE project. The spectrometer is also

5. Emittance

The beam emittance is a qualitative way of describing the quality of the beam, essentially, it is a measure of how parallel the particles of the beam are to each other. It is a conserved quantity in the absence of a z component (i.e. in the direction of the beam) in the magnetic field and when the beam is not being accelerated.

The state of a beam can be described by it's position and velocity, so each particle in the beam is represented in six-dimensional phase space with coordinates (x, p_x, y, p_y, z, p_z) where p is the momentum in it's respective direction. For very small where $p_x \approx\ p_0 x'$ and $p_y \approx\ p_0 y'$ are the transverse momenta, z is the position along the beam trajectory, p_z is the longitudinal momentum and x' and y' are the trajectory angles to the horizontal and vertical planes. Since the transverse momenta, and therefore x' and y', are generally quite small we can approximate $\sin(x') \approx x'$ and $\sin(y') \approx y'$. We can then project this six-dimensional volume into three independent two-dimensional phase planes, because in this approximation there is no coupling between those degrees of freedom.

The horizontal emittance of the beam is defined by considering the ellipse in the $x' - x$ phase space that contains

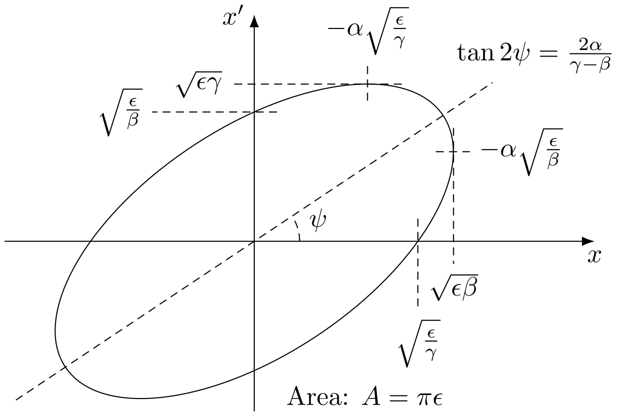

Figure 2: Graphical representation of the relation between the twiss parameters [17]

95% of all the particles [16]. The area contained by this ellipse divided by π is defined as the emittance in units of π-mm-mrad.

$$\int_{\text{ellipse}} \mathrm{d}x\mathrm{d}x' = \pi\epsilon \tag{1}$$

Fig. 2 shows a beam projected onto a two dimensional phase plane. The emittance can be described by the equation of the ellipse:

$$\gamma x^2 + 2\alpha x x' + \beta x'^2 = \epsilon \tag{2}$$

where α, β are γ are ellipse parameters that determine the ellipse's shape and orientation and are related by this equation

$$\beta\gamma - \alpha^2 = 1 \tag{3}$$

It follows that the beam matrix is

$$\sigma = \begin{pmatrix} \sigma_{1,1} & \sigma_{1,2} \\ \sigma_{2,1} & \sigma_{2,2} \end{pmatrix} = \begin{pmatrix} \beta\epsilon^2 & -\alpha\epsilon^2 \\ -\alpha\epsilon^2 & \gamma\epsilon^2 \end{pmatrix} \tag{4}$$

such that $\epsilon = \det\sigma$, $\sigma_{1,1}$ is the besm size and $\sigma_{1,2}$ is the orientation in phase space.

6. The Simulation

The simulation of this experiment was split into three logical parts: the simulation of the beam, the background and camera readout simulation, and the reconstruction of the beam. It is designed such that each part of the code is able to act independently.

6.1. The Electron Beam

Given enough computing power and time, the simulation of the beam exiting the plasma cell, passing through two quadrupoles and through a dipole could have been done on BDSIM [18], a Geant4 [19] toolkit for simulating radiation traveling through an accelerator. This software package simulates a single particle at a time, updating it's position and velocity at each step through the accelerator, applying the effect of forces from all fields within the accelerator. For beams consisting of 1×10^9 particles, tracking each particle individually as they travel down the beam line would take large amounts of time using the available computing power.

Parameter	Expected value
Emittance ϵ	1×10^{-6} m rad
β	1
α	0.5
Mean energy $\bar{E}$	1.3 GeV
Energy spread σ_E	0.4 GeV
N. electrons N_{e^-}	1×10^9
Bg. photons	1×10^5 m^{-2}

Table 1: The expected values for many experimental parameters have been calculated. It should be noted that these values are missing error values. It can be assumed that the error on each value can be given by half the least significant digit.

A new program was written, taking advantage of beam matrices to describe the beam as a whole. The goal of the first part of this program is to simulate the intensity of the incident beam at each pixel on the screen.

6.1.1. BDSIM calibration

The effect of the quadrupole and the dipole are dependant on the energy of the individual electrons in the beam.

So to calculate the energy and number of an electrons as a function of the horizontal screen position a number of BDSIM simulations were run. 100 000 single electrons where fired down the AWAKE beam line. These electrons had a square energy distribution from 0 to 10 TeV, and had a gaussian spacial distribution with $\sigma_x = \sigma_y = 6$ mm, and no transverse momentum meaning zero emittance. These were used to plot the functions in Figures **??** and 3b.

6.1.2. Deriving the Beam Size Function

The dipole spreads the beam such that the electrons in each vertical strip of pixels can be grouped together and their energy approximated to be equal, as the energy spread in each strip will always be less than 0.5 %. This was calculated from Figure 3a by dividing the difference in energies between adjacent strips by the energy value at that strip for all strips and the maximum value was 0.5 %.

The root mean square of the vertical beam size on the screen can be extracted from the resultant beam matrix σ_1. To arrive at this beam matrix, the transport matrix $\mathcal{M}$ is applied to the initial beam matrix σ_0. The transport matrix is the product of the transport matrices for each component of the spectrometer:

$$\mathcal{M} = \mathcal{M}_d(d) \cdot \mathcal{M}_{QD}(l_2) \cdot \mathcal{M}_d(g_2) \cdot \mathcal{M}_{QF}(l_1) \cdot \mathcal{M}_d(g_1) \tag{5}$$

The beam matrix element $\sigma_{11} = \langle y \rangle^2 = \epsilon\beta$

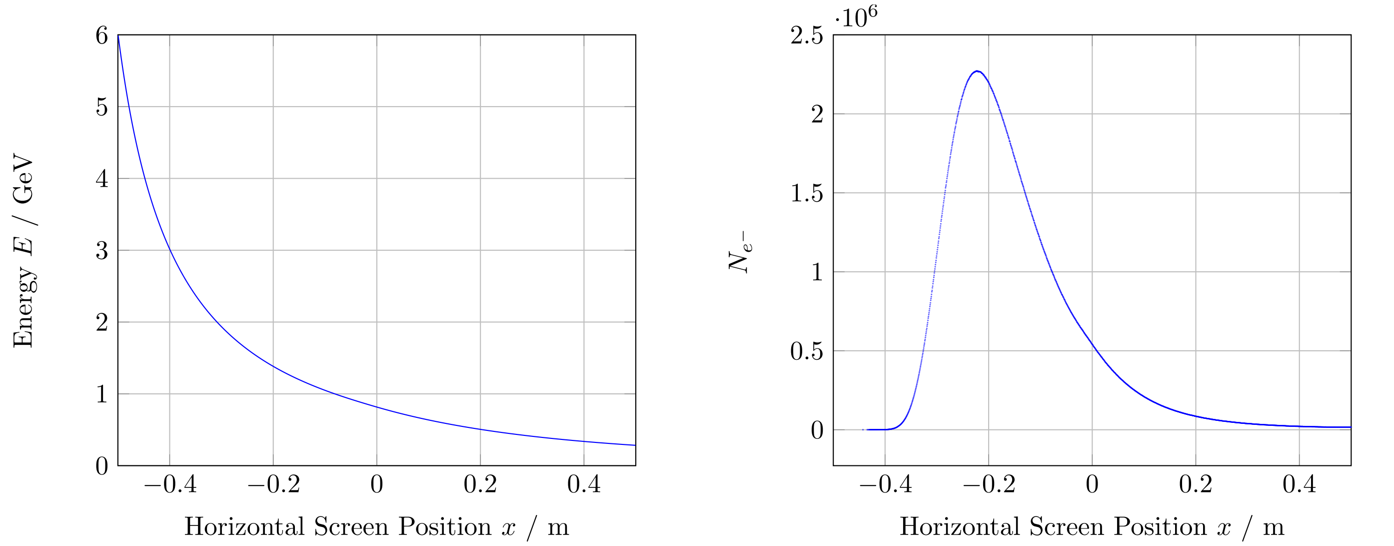

(a) The corresponding electron energies for each vertical pixel strip.

(b) The number of electrons expected to hit the screen at each x position. (Expected experimental parameters used)

Figure 3: The functions $E(x)$ and $N_{e^-}(x)$ extracted from the BDSIM callibration output data. These functions are used to calculate the horizontal spread of the electrons across the screen.

Applying the matrix multiplication results in the vertical beam size as a function of the horizontal screen position:

$$\sigma_y^2 = \sigma_{1,11} = C^2(x)\sigma_{0,11} + 2C(x)S(x)\sigma_{0,12} + S^2(x)\sigma_{0,22} \tag{6}$$

After generating, a two dimensional histogram representing the number of electrons hitting the screen at each pixel the goal is to simulate the effectiveness of the equipment and translate this number to represent the raw signal that will be read off for each pixel.

6.2. Backgrounds

How good the measurement of the emittance is, is most dependant on the magnitude of the multiple sources of backgrounds as well as the reliability of the equipment. The following sources of error were taken into account: the efficiency of the scintillator screen, the acceptance of the camera, the background photon density, the emittance of photoelectrons, the thermal noise, the microchannel plate (MCP) and the readout noise. Each source of noise is added to each pixel independently.

The first two error sources, the scintillator screen and the camera acceptance, both scale the signal. So for each electron that hits the screen, it is expected that an average of 5000 [] photons are to be emitted. The camera acceptance, is the ratio of photons that the camera registers to the number of photons emitted by the scintillator, with a value of 1.5×10^{-5}. After the addition of these two effects, the camera is expected to receive 7.5 % of the original electron signal. The expected value for the number of photons incident on the camera due to the beam electrons is a Poisson random number.

It is assumed that there is a uniform distribution of photons incident on the camera. The density of these electrons is expected to be $1 \times 10^5\,\mathrm{m}^{-2}$ equating to 0.01 background photons per pixel during the 3×10^{-3} s the gate is open. This is a discrete value, and so is also a Poisson random number. As discussed later in Section 7 this value is very small in comparison to the signal produced by the beam and will only have an effect if the density of background photons is multiple magnitudes larger than the expected value.

The camera's photomultipliers then convert the photons of light back to an electrical current. This multiplies the incident number of photons by the quantum efficiency of the camera, 0.15. thermal photoelectrons per pixel per second is expected to be 0.016 [20], with the camera running at the expected temperature of −30 °C with 16 °C cooling water and an ambient room temperature of 16 °C. This value is typically doubles for each 5 °C rise in temperature of the camera [20]. At these running temperatures of the camera, about 9 photoelectrons are expected to be generated during the time the gate is open, which is an insignificant proportion in comparison to the beam signal, creating 1×10^7 photoelectrons before MCP amplification.

The microchannel plate amplifies the number of photoelectrons by 1442 amplifying all previously added backgrounds. This was simulated by simply scaling the value of the bin by this value rather than generating a Poisson random number centred about this value.

And finally, before the values of the signal is obtained, a readout noise is added. This background is expected to add 7.2 readout electrons per image pixel for the camera operating at 1 MHz.

6.2.1. Error Calculations

Poisson statistics were used for the calculation of errors. Once the shape of the incident beam on the screen was calculated the number of electrons incident on each pixel was given an error of the square root of the count. Two methods of error propagation were used depending on the nature of the process involved. The following processes were modeled as additive processes: background photons hitting the screen, the thermal electrons from the currents in the camera and the readout noise, whereas the multiplicative processes are: photon generation at the scintilator screen, photoelectron generation in the camera PMTs and the amplification of the electron signal by the MCP.

Basic error propagation techniques were used here. For the additive processes, where the new value of each bin n is the sum between the old bin value n_0 and the value given by the process n_{proc}: $n = n_0 + n_{\text{proc}}$ the propagation of error is given by calculating the hypotenuse of the absolute errors:

$$\Delta n = \sqrt{\Delta n_0^2 + \Delta n_{\text{proc}}^2} \tag{7}$$

where the error of a Poisson random number is the square root of the value.

For the multiplicative processes, i.e. $n = \lambda_{\text{proc}} n_0$ where λ_{proc} is the scaling factor of the process the propagation of the error is given by calculating the hypotenuse of the percentage errors:

$$\Delta n = n\sqrt{\left(\frac{\Delta n_0}{n_0}\right)^2 + \left(\frac{\Delta \lambda_{\text{proc}}}{\lambda_{\text{proc}}}\right)^2} \tag{8}$$

$$\Delta n = n\sqrt{\left(\frac{\sqrt{n_0}}{n_0}\right)^2 + \left(\frac{\sqrt{n}}{n}\right)^2} \tag{9}$$

Many of the errors Δn_{proc} and $\Delta \lambda_{\text{proc}}$ were missing at the time of simulation. All background noises are modeled as uniformly distributed Poisson random numbers so the associated error on each value can correctly be calculated (under these assumptions) to be the square root of the value. However for multiplicative processes

6.3. Calculating the Emittance

The signal received from the camera is required to be scaled back, and background noises removed. This is done by tracing the beam backwards and subtracting or dividing

The vertical beam size function used to simulate the shape of the incident electron beam is then fit to the measured beam sizes. The fitting is done wholly by CERN ROOT's χ^2 minimising fitting algorithm [21], using the three beam parameters ϵ, β and γ as parameters to be minimised.

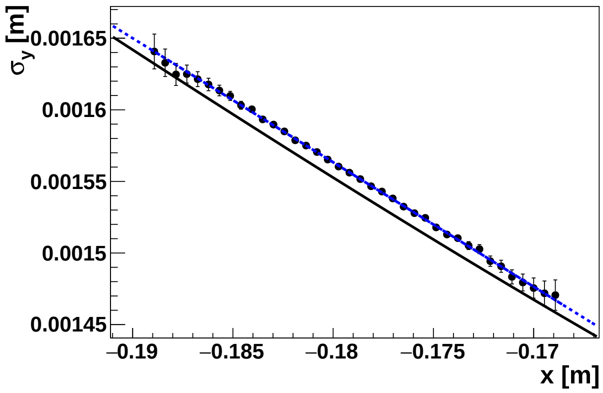

Figure 4: Blue line representing the reconstruction of the shape of the beam that hits the screen consistently overestimates the vertical beam size. This run used a small percentage energy spread of 1 %. With all other parameters set to their expected value.

7. Results

7.1. The Output Plot

Along with the χ^2 minimised parameter values of the fit, each simulation generated a plot, showing the simulated, measured and fitted vertical beam size functions as a function of horizontal position x on the screen. Figure 4 is an output plot for a run with a small (1 %) energy spread. The solid black line is the shape of the simulated electron beam that hits the screen, the black points show the simulated measurements of the RMS width of the fitted gausian for each vertical strip of pixels. The blue dashed line is the beam size function fitted to the points.

7.2. Binning errors

After the investigation of multiple experimental parameters, the emittance measurement consistently converged to a value 1×10^{-8} larger than the input emittance. The reason for this systematic error was found to be due to the discritisation of the beam hitting the screen meaning that the measurement of the vertical beam size was consistently overestimated. Since the electrons in each pixel are not uniformly distributed but rather more densely distributed closer towards the mean value, giving rise to a systematic overestimation of the vertical beam size of up to two times the vertical size of the pixel. This effect can be seen most clearly when a very small energy spread was used as can be seen in Figure 4, where the measured beam heights are consistently larger than the actual beam height.

7.3. Energy Spread

Initially, the mean energy of the beam and energy spread of the beam were tested independently. Simulations for all combinations of the following energies $E \in \{0.5, 1, 1.3, 2.0, 3.05.0\}$ and the following energy spreads $\sigma_E \in \{0.01, 0.1, 0.3, 0.4\}$ were run. These energies and

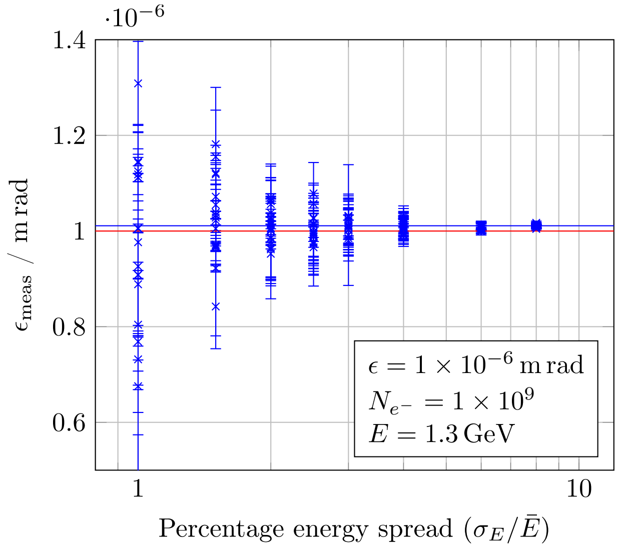

(a) Plot of the simulated emittance measurement against the percentage spread of beam energy.

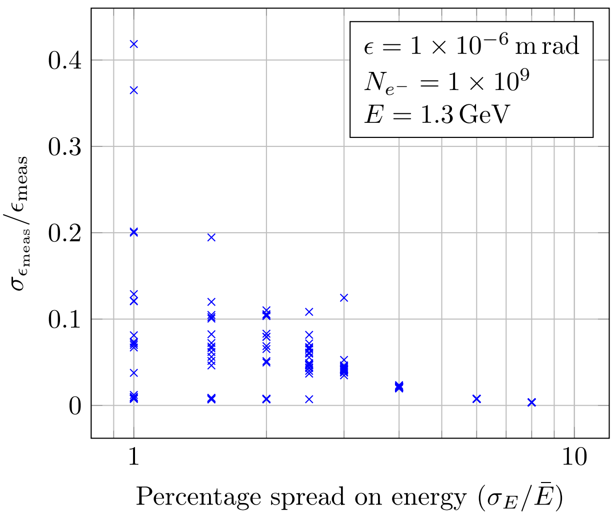

(b)

energy spreads were chosen such that at least one standard deviation of the beam hit the screen. As Figure 3a shows, the range of energies that hit the screen for the is from ∼0.28 to 6 GeV.

The estimated energy spread of the electron beam is 0.4 GeV,

It was found that the error of the measurement of the emittance

Mean beam energies tested ranged from 0.1 to 4 GeV

7.4. Input Emittance

Since the emittance

7.5. Background Photons

8. Conclusion

8.1. Errors

Despite accpeting the error bars for many of the graphs, it is still likely that the calculation of the errors are wrong. Looking at the output files of simulations with very large backgrounds, it is clear that the error bars do not take into account the large statistical fluctuations about the expected beam size. The calculation of errors in the simulation is well understood appart from the calculation of the error of the χ^2 fitted parameters.

8.2. Parameters

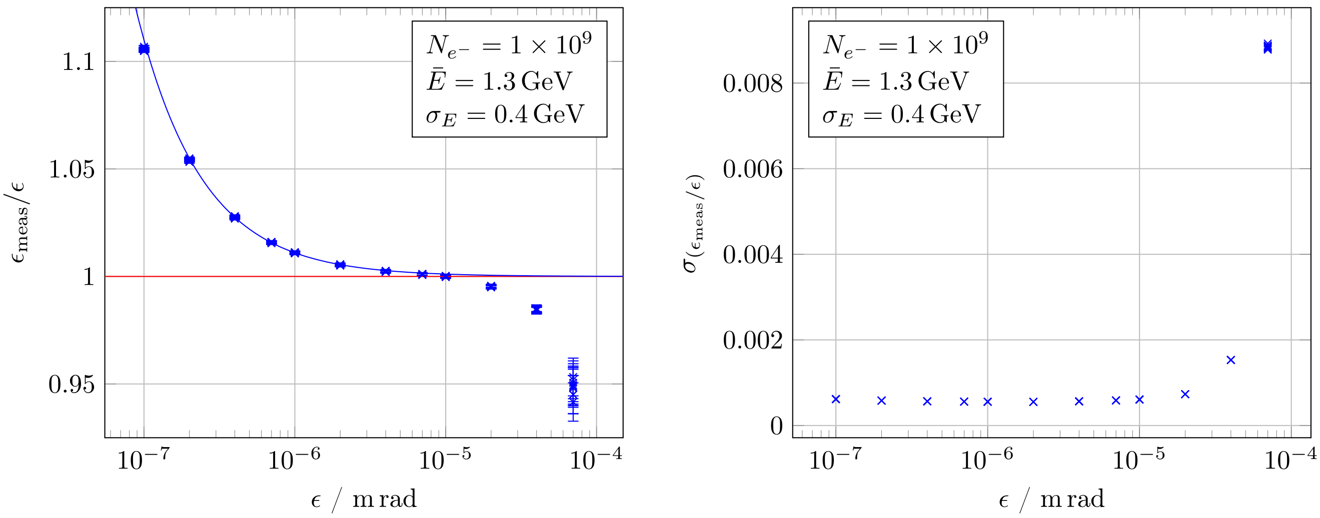

(a) (b)

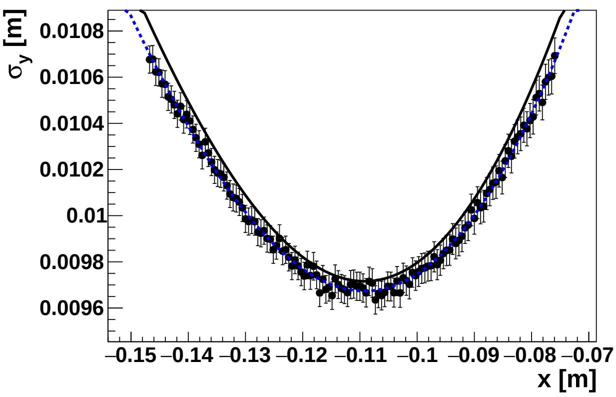

Figure 7: Beam reconstruction for an input emittance of 7×10^{-5} showing the underestimation of the measured vertical beam sizes.

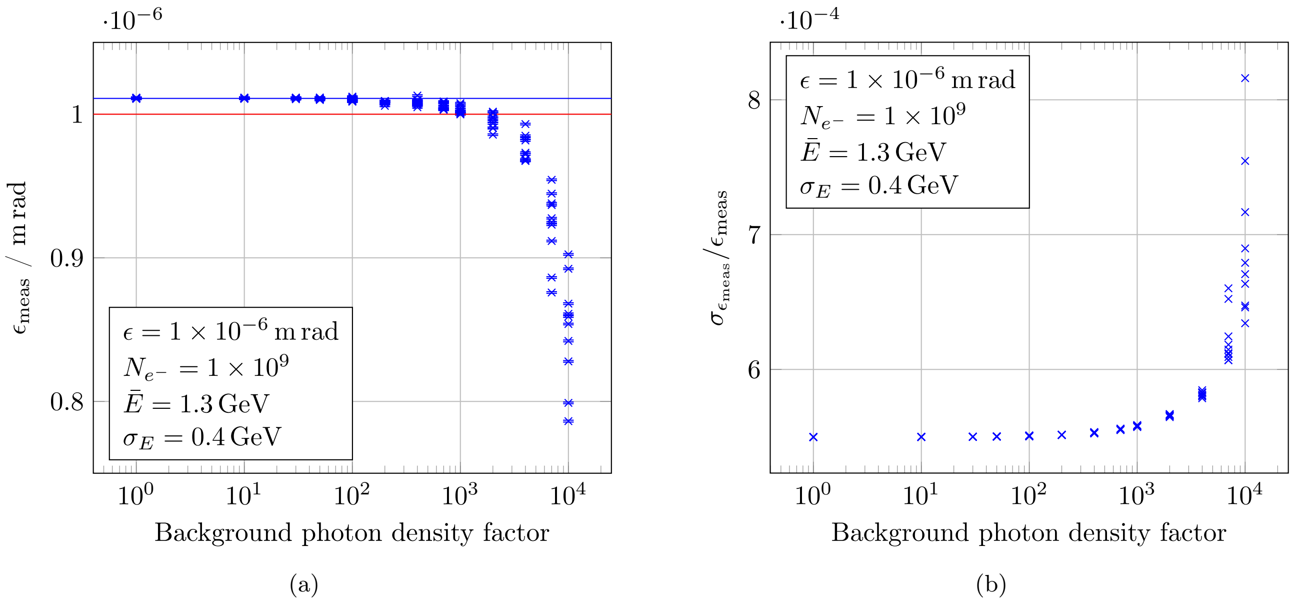

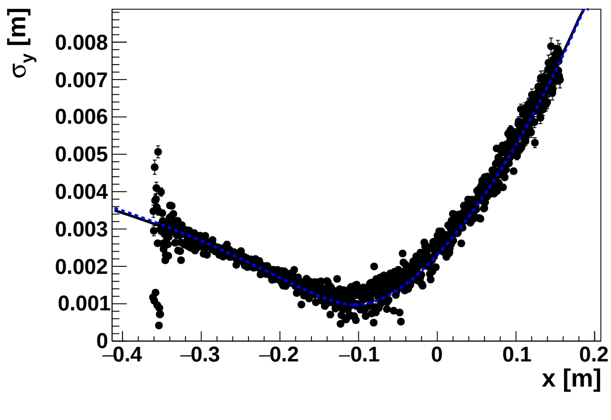

Figure 9: Beam reconstruction for a large background.

References

[1] C. O'Luanaigh, "First images of collisions at 13 tev," May 2015.

[2] R. Barate *et al.*, "Search for the standard model Higgs boson at LEP," *Phys. Lett.*, vol. B565, pp. 61–75, 2003.

[3] T. Tajima and J. M. Dawson, "Laser electron accelerator," *Phys. Rev. Lett.*, vol. 43, pp. 267–270, 1979.

[4] W. Lu, M. Tzoufras, C. Joshi, F. S. Tsung, W. B. Mori, J. Vieria, R. A. Fonseca, and L. O. Silva, "Generating multi-GeV electron bunches using single stage laser wakefield acceleration in a 3D nonlinear regime," *Phys. Rev. ST Accel. Beams*, vol. 10, p. 061301, 2007.

[5] W. P. Leemans, B. Nagler, A. J. Gonsalves, C. Toth, K. Nakamura, C. G. R. Geddes, E. Esarey, C. B. Schroeder, and S. M. Hooker, "GeV electron beams from a cm-scale accelerator," *Nature Phys.*, vol. 2, pp. 696–699, 2006.

[6] N. Kumar, A. Pukhov, and K. Lotov, "Self-modulation instability of a long proton bunch in plasmas," *Physical review letters*, vol. 104, no. 25, p. 255003, 2010.

[7] K. Lotov, G. Lotova, V. Lotov, A. Upadhyay, T. Tückmantel, A. Pukhov, and A. Caldwell, "Natural noise and external wakefield seeding in a proton-driven plasma accelerator," *Physical Review Special Topics-Accelerators and Beams*, vol. 16, no. 4, p. 041301, 2013.

[8] C. Siemon, V. Khudik, S. A. Yi, A. Pukhov, and G. Shvets, "Laser-seeded modulation instability in a proton driver plasma wakefield accelerator," *Physics of Plasmas (1994-present)*, vol. 20, no. 10, p. 103111, 2013.

[9] J. Vieira, W. Mori, and P. Muggli, "Hosing instability suppression in self-modulated plasma wakefields," *Physical Review Letters*, vol. 112, no. 20, p. 205001, 2014.

[10] H. Wiedemann *et al.*, *Particle accelerator physics*, vol. 314. Springer, 2007.

[11] E. Öz and P. Muggli, "A novel rb vapor plasma source for plasma wakefield accelerators," *Nuclear Instruments and Methods in Physics Research Section A: Accelerators, Spectrometers, Detectors and Associated Equipment*, vol. 740, pp. 197–202, 2014.

[12] E. Öz, F. Batsch, and P. Muggli, "A Novel Laser Ionized Rb Plasma Source for Plasma Wakefield Accelerators," in *Proceedings, 5th International Particle Accelerator Conference (IPAC 2014): Dresden, Germany, June 15-20, 2014*, p. TUPME073, 2014.

[13] J. Vieira, R. A. Fonseca, W. B. Mori, and L. O. Silva, "The ion motion in self-modulated plasma wakefield accelerators," *Phys. Rev. Lett.*, vol. 109, p. 145005, 2012.

[14] J. Vieira, R. A. Fonseca, W. B. Mori, and L. O. Silva, "Ion motion in the wake driven by long particle bunches in plasmas," *Phys. Plasmas*, vol. 21, p. 056705, 2014.

[15] E. Gschwendtner *et al.*, "AWAKE, The Advanced Proton Driven Plasma Wakefield Acceleration Experiment at CERN," *Nucl. Instrum. Meth.*, vol. A829, pp. 76–82, 2016.

[16] J. Buon, "Beam phase space and emittance," *CERN European Organization for Nuclear Research-Reports-CERN*, pp. 89–89, 1994.

[17] A. Caldwell *et al.*, "Path to AWAKE: Evolution of the concept," *Nucl. Instrum. Meth.*, vol. A829, pp. 3–16, 2016.

[18] I. Agapov, G. Blair, S. Malton, and L. Deacon, "Bdsim: A particle tracking code for accelerator beam-line simulations including particle–matter interactions," *Nuclear Instruments and Methods in Physics Research Section A: Accelerators, Spectrometers, Detectors and Associated Equipment*, vol. 606, no. 3, pp. 708–712, 2009.

[19] S. Agostinelli, J. Allison, K. a. Amako, J. Apostolakis, H. Araujo, P. Arce, M. Asai, D. Axen, S. Banerjee, G. Barrand, *et al.*, "Geant4 - a simulation toolkit," *Nuclear instruments and methods in physics research section A: Accelerators, Spectrometers, Detectors and Associated Equipment*, vol. 506, no. 3, pp. 250–303, 2003.

[20] ANDOR an Oxford Instruments company, Andor Technology Ltd., 7 Millennium Way, Springvale Business Park, Belfast, BT12 7AL, Northern Ireland, *Hardware Guide for the iStar Intensified sCMOS camera*, Sep 2016.

[21] R. Brun and F. Rademakers, "ROOT: An object oriented data analysis framework," *Nucl. Instrum. Meth.*, vol. A389, pp. 81–86, 1997.